http://dx.doi.org/10.5012/bkcs.2012.33.11.3719

Contribution of Counterion Entropy to the Salt-Induced Transition Between B-DNA and Z-DNA

Youn-Kyoung Lee, Juyong Lee, Jung Hyun Choi, and Chaok Seok*

*Department of Chemistry, Seoul National University, Seoul 151-747, Korea. *E-mail: chaok@snu.ac.kr*
Received August 11, 2012, Accepted August 14, 2012

Formation of Z-DNA, a left-handed double helix, from B-DNA, the canonical right-handed double helix, occurs during important biological processes such as gene expression and DNA transcription. Such B-Z transitions can also be induced by high salt concentration *in vitro*, but the changes in the relative stability of B-DNA and Z-DNA with salt concentration have not been fully explained despite numerous attempts. For example, electrostatic effects alone could not account for salt-induced B-Z transitions in previous studies. In this paper, we propose that the B-Z transition can be explained if counterion entropy is considered along with the electrostatic interactions. This can be achieved by conducting all-atom, explicit-solvent MD simulations followed by MM-PBSA and molecular DFT calculations. Our MD simulations show that counterions tend to bind at specific sites in B-DNA and Z-DNA, and that more ions cluster near Z-DNA than near B-DNA. Moreover, the difference in counterion ordering near B-DNA and Z-DNA is larger at a low salt concentration than at a high concentration. The results imply that the exclusion of counterions by Z-DNA-binding proteins may facilitate Z-DNA formation under physiological conditions.

Key Words : Z-DNA, B-Z transition, MM-PBSA, Classical density functional theory, Counterion entropy

Introduction

Z-DNA, a non-canonical, left-handed form of the DNA double helix, is one of the biologically active DNA conformations along with B-DNA and A-DNA.[1,2] Z-DNA formation is highly correlated with negative superhelical strain induced during the transcription process.[2-4] A report by Takaoka *et al.* that a putative Z-DNA binding protein, DAI, is related to immune responses makes the Z-DNA conformation of more interest to researchers.[5] Moreover, a relationship between Z-DNA and cancer has been suggested since 1980's.[6-8]

Transition from B-DNA to Z-DNA occurs at high salt concentrations *in vitro* for some sequences of DNA,[9,10] and several theoretical studies have attempted to describe that phenomenon.[11-17] Although molecular dynamics (MD) simulations of all-atom representations of DNA and its solvent environment may be able to provide a detailed description of the system, convergence problems in the huge configuration space limit the application of this approach in the calculation of DNA free energy in a solution.[18]

Other approaches such as mean-field electrostatic theories that adopt a continuum solvent model[15,16,19] have also been employed. Those studies emphasized the strong electrostatic repulsion between proximate phosphate groups in Z-DNA and suggested more effective screening of the repulsion under higher salt concentrations.[11,12,15,19] In addition, 3D-RISM approach, a thermodynamic integral equation method, qualitatively explains the changes in the relative stability of B-DNA and Z-DNA with changes in salt concentration.[11] That study concluded that solvation free energy from salt ions is an important contributor to the B-Z transition.

In this study, all-atom MD simulations of the B-DNA and Z-DNA forms of the sequence $[d(CGCGCGCGCGCG)]_2$ in 0.1 M and 5 M NaCl solutions were conducted with explicit water and explicit ions in order to investigate contributions of different free energy components to the B-Z transition at low and high salt concentrations. The free energy of the DNA solutions was estimated by MM-PBSA (molecular mechanics-Poisson-Boltzmann surface area) and molecular DFT (density functional theory) methods. Our MM-PBSA calculation shows that the free energy contribution from electrostatic interactions alone favors Z-DNA at both low and high salt concentrations, supporting previous nonlinear PB calculations.[19] However, the contribution of counterion entropy, which is not considered by MM-PBSA but is estimated by molecular DFT, favors B-DNA at both low and high salt concentrations. This is because the entropy loss, due to counterion ordering around DNA, is smaller in B-DNA solutions. The degree of counterion ordering is significantly different for B-DNA and Z-DNA at low concentration, but the difference becomes smaller at high concentration. The total free energy, *i.e.*, the sum of MM-PBSA free energy and counterion entropy, explains the changes in the relative stability of B-DNA and Z-DNA with salt concentration.

Thus, the current study suggests that both electrostatic interactions and counterion entropy play important roles in determining the relative stability of B-DNA and Z-DNA. Experiments on the conformational transition of Z-DNA to B-DNA induced by heating at high salt concentrations support the suggested importance of entropy.[17,20-22] In addition, counterion entropy is expected to be partly responsible for the occurrence of the B-Z transition in solutions containing

higher-valent counterions at lower salt concentrations involving a smaller counterion entropy loss. The free energy calculated from integral equation theories, such as 3D-RISM,[11] elegantly incorporates the contributions from counterion entropy and electrostatics; however, separating the two contributions is not trivial.

Our MD simulation trajectories for B-DNA and Z-DNA provide interesting detail on their structural features which is in agreement with the results in previous experimental and theoretical studies,[23,24] providing justification for the use of the MD trajectories in the free energy analysis described above although application of the PB model to nucleic acid systems is still expected to be a source of error.[25-27]

Methods

All-Atom, Explicit Water Molecular Dynamics Simulations for B-DNA and Z-DNA. We performed MD simulations on four systems, B-DNA and Z-DNA separately in 0.1 M and 5 M NaCl solutions, to investigate the free energy components contributing to the relative stability of B-DNA and Z-DNA. A dodecamer DNA duplex with the sequence $[d(CGCGCGCGCGCG)]_2$ was employed for both B-DNA and Z-DNA simulations because a CG-repeat is reported to favor Z-DNA formation. The twelve-nucleotide-pair segment was chosen as it covers at least a single double helix turn in both B-DNA and Z-DNA.

The initial structure for B-DNA was created using the NUCGEN[28] module of the AMBER10 software package. For Z-DNA, the 3ZNA model structure deposited in the Protein Data Bank[29] was used as the initial structure. For each simulation, water molecules (6421 for B-DNA and 7284 for Z-DNA at 0.1 M, and 7466 for B-DNA and 8008 for Z-DNA at 5 M) were added to produce a minimum distance of 12 Å from the solute to the truncated octahedral simulation box boundaries. Sodium or chloride ions were added to neutralize the system and to acquire the desired salt concentrations.

All simulations were carried out using AMBER10 software.[30] Within AMBER10, the standard parmbsc0 force field[31] was used to describe the energetics of DNA, together with the TIP3P water model and the ions08 ion model.[32] The particle mesh Ewald method[33] was employed to treat the long-range electrostatics under periodic boundary conditions. The non-bonded cutoff for long-range interactions was set to 10 Å, and a time step of 2 fs was used by constraining the bond lengths of hydrogen atoms with SHAKE.

Each of the four DNA-salt systems was prepared by initial energy minimization and subsequent heating to 300 K applying harmonic restraints on the DNA atoms with a force constant of 2 kcal/Å^2·mol. An unrestrained 1-ns equilibration MD simulation at 300 K under 1 atm followed. A Langevin thermostat with a collision frequency of 2.5 ps^{-1} and a weak-coupling-based barostat[34] with a 2.0 ps relaxation time were employed. Production MD simulation was carried out for 45 ns for each system.

Analysis of DNA Conformations. DNA conformational parameters were calculated using CURVES+ (http://gbio-pbil.ibcp.fr/Curves_plus/Curves+.html)[35], and conformational changes in B-DNA and Z-DNA related to salt concentration were examined. Details are described in Supporting Information.

Free Energy of B-DNA and Z-DNA Estimated with MM-PBSA. The MM-PBSA technique was used to estimate the free energy of B-DNA and Z-DNA in solutions of two different salt concentrations and to determine the contributions of different free energy components to their relative stability. The free energy at temperature T corresponding to a state represented by a snapshot of a solvated DNA is expressed as

$$G_{\mathrm{DNA}}^{\mathrm{Sanpshot}} = H_{\mathrm{int}} + H_{\mathrm{vdW}} + H_{\mathrm{Coul}} + G_{\mathrm{PB}} + G_{\mathrm{SA}} - TS\,, \qquad (1)$$

where H_{int}, H_{vdW}, and H_{Coul} denote the DNA internal strain energy, van der Waals energy, and Coulomb electrostatic energy, respectively. The term G_{PB} is the polar solvation free energy value calculated from the Poisson-Boltzmann (PB) method using the AMBER10 PBSA solver with default parameters.[36] The term G_{SA} is the non-polar solvation free energy value and is approximately proportional to the solvent accessible surface area, SA.[37] The entropy, S, consists of the translational, rotational, and vibrational entropies of the solute and was calculated with the AMBER10 *nmode* module. The DNA free energy was then calculated as $G_{\mathrm{DNA}} = \langle G_{\mathrm{DNA}}^{\mathrm{Sanpshot}} \rangle$, where $\langle G_{\mathrm{DNA}}^{\mathrm{Sanpshot}} \rangle$ is the average of the $\langle G_{\mathrm{DNA}}^{\mathrm{Sanpshot}} \rangle$ value from 1500 snapshots collected every 30 ps during the 45-ns simulations. Contributions from each enthalpy and entropy component to the free energy are obtained by similarly averaging each term on the right-hand side of Eq. (1).

Nucleotide pair-wise energy decomposition analysis was carried out using the *mm_pbsa.pl* and *mm_pbsa_statistics.pl* scripts in AMBER10. Details are described in Supporting Information.

Counterion Entropy Estimated with Molecular Density Functional Theory. The counterion distributions obtained from the above B-DNA and Z-DNA simulations differed significantly, and the size of the difference varied with salt concentration. That implies that counterion free energy, especially counterion entropy, may contribute to the relative stability of B-DNA and Z-DNA. Although the contribution of counterions to the solvation free energy of DNA is considered in the MM-PBSA calculation partly by the mean field approximation, counterion entropy resulting from ion ordering around the DNA and the free energy contribution due to ion-ion interactions are not considered by MM-PBSA.

However, such contributions to the free energy may be estimated by applying molecular density functional theory (DFT), if an appropriate free energy functional can be found. Molecular DFT has been applied to the study of inhomogeneous liquid or solid systems such as those involving interfaces between two different phases.[38,39] Density functional theory for such systems is most easily described in the grand canonical ensemble at fixed chemical potential μ,

volume V, and temperature T. The grand potential for a homogeneous system is $\Omega = -pV$, where p is the pressure. It is related to the Helmholtz free energy through the Legendre transformation $\Omega = F - \mu N$. The thermodynamic potential of current interest is the Gibbs free energy G at constant number of counterions N, pressure p, and temperature T. G is related to the grand potential through the Legendre transformation $G = \Omega + \mu N + pV$. The counterion Gibbs free energy of the B-DNA and Z-DNA systems with the same bulk counterion density ρ_0 are $G_B^{ion} = \Omega_B^{ion} + \mu(\rho_0)N + pV_B$ and $G_Z^{ion} = \Omega_Z^{ion} + \mu(\rho_0)N + pV_Z$, respectively. Therefore, $\Delta G^{ion} = G_Z^{ion} - G_B^{ion} = \Omega_Z^{ion} - \Omega_B^{ion}$, where the $p(V_Z - V_B)$ is assumed small (it also corresponds to the difference between the Helmholtz free energy and the Gibbs free energy).

The grand potential for an inhomogeneous system of counterion density $\rho(\mathbf{r})$, which is a function of the spatial coordinate $\mathbf{r}$, is expressed as[38,39]

$$\Omega^{ion}[\rho(\mathbf{r})] = F^{ion}[\rho(\mathbf{r})] - \mu \int d\mathbf{r}\rho(\mathbf{r}) . \quad (2)$$

The counterion Helmholtz free energy $F^{ion}[\rho(\mathbf{r})]$ can be expressed as a unique functional of counterion density as follows[38,39]

$$F^{ion}[\rho(\mathbf{r})] = F_{ideal}^{ion}[\rho(\mathbf{r})] + F_{excess}^{ion}[\rho(\mathbf{r})] , \quad (3)$$

where $F_{ideal}^{ion}[\rho(\mathbf{r})]$ represents the free energy functional of a non-interacting (thus called "ideal") inhomogeneous ion solution under an effective external field that gives rise to the given density, and where $F_{excess}^{ion}[\rho(\mathbf{r})]$ is the excess free energy functional not taken into account by $F_{ideal}^{ion}[\rho(\mathbf{r})]$.

The ideal free energy functional is shown as[40]

$$F_{ideal}^{ion}[\rho(\mathbf{r})] = k_B T \int d\mathbf{r}\rho(\mathbf{r})[\ln\{\lambda^3\rho(\mathbf{r})\} - 1] , \quad (4)$$

where k_B is the Boltzmann constant, T is the absolute temperature, $\lambda = (h^2/2k_BTm\pi)^{1/2}$ is the thermal de Broglie wavelength of the ion, h is the Planck constant, and m is the mass of the ion. The form of the ideal free energy functional in Eq. (4) reminds the common formula for entropy, and the entropy due to counterion ordering is a major contributor to this term. Ion-ion and ion-DNA interactions also contribute to this term effectively by giving rise to the current density profile.

For the excess free energy functional, a free energy functional expansion around the state of homogeneous ion density ρ_0 may be used, as[40]

$$F_{excess}^{ion}[\rho(\mathbf{r})] = F_{excess}^{ion}[\rho_0] + \int d\mathbf{r}_1 \left(\frac{\delta F_{excess}^{ion}}{\delta\rho(\mathbf{r}_1)}\right)_{\rho_0} (\rho(\mathbf{r}_1) - \rho_0) + \frac{1}{2}\int d\mathbf{r}_1 d\mathbf{r}_2 \left(\frac{\delta^2 F_{excess}^{ion}}{\delta\rho(\mathbf{r}_1)\delta\rho(\mathbf{r}_2)}\right)_{\rho_0} (\rho(\mathbf{r}_1) - \rho_0)(\rho(\mathbf{r}_2) - \rho_0) + \cdots \quad (5)$$

where, the zeroth order term, $F_{excess}^{ion}[\rho_0]$, is constant; thus is the same for B-DNA and Z-DNA. Here, the counterion free energy is calculated from the ideal free energy functional given by Eq. (4), and that approach considers up to the zeroth order term of the excess free energy functional.

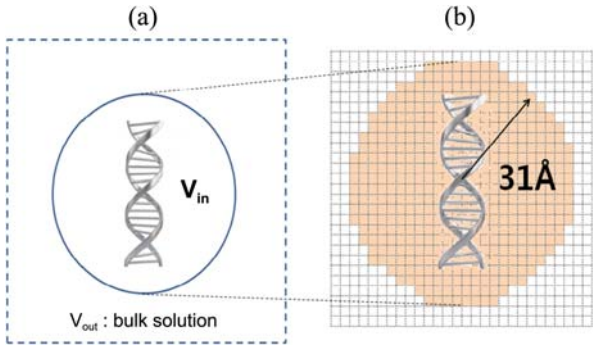

Figure 1. Schematic images of the DNA systems prepared for the calculation of counterion free energy. Within simulation box, a sphere of radius 31 Å is created and then immersed in a bulk solution of ion density ρ_0 as in (a). The volume of the sphere is denoted by V_{in}, and the volume outside the sphere by V_{out}. The counterion density profile $\rho(\mathbf{r})$ is obtained from the counterion trajectories from MD simulations on 1.0 Å^3 cubic boxes within the cubic Cartesian grid, as illustrated in 2D for a B-DNA solution in (b).

For such DFT calculation, an appropriate representation of ion density is necessary. We obtained a discrete ion distribution by counting the number of ions in each cubic cell of size 1.0 Å^3 on three dimensional grid points after reorienting the 4,500 MD snapshots of the 45-ns simulation to superpose DNA. To smooth the density distribution, the local ion density of 3^3 cells was averaged for the center cell. Finally, the system was extended to infinite volume by immersing a finite sphere from the simulation box (centered at the midpoint of the DNA helical axis) in a bulk solution of homogeneous ion concentration, as shown schematically in Figure 1. The radius of the sphere was determined to be 31 Å at which the density distribution profile reaches a plateau.

The boundary density of a B-DNA solution is slightly different from that of a Z-DNA solution when prepared to have the same 'average' ion density, because the degree of counterion ordering near B-DNA is different from the ordering near Z-DNA. We would like to compare the free energy in B-DNA and Z-DNA for the same bulk ion concentration, but it is impractical to know beforehand how many ions are needed to meet such condition exactly. Therefore, the counterion density of the B-DNA solution was scaled to that of Z-DNA by multiplying by a constant value, assuming that counterion free energy does not change markedly over the relevant concentration range. As a result, the density of the B-DNA solution was scaled by 0.83 at the 0.1 M concentration and by 1.00065 at the 5 M concentration. The exact bulk density values prepared in this way are 0.12 M and 5.2 M for low and high salt concentration solutions, respectively.

The Gibbs free energy difference between the B-DNA and Z-DNA solutions is then calculated as follows:

$$\Delta G^{ion} = F_{ideal}^{ion}[\rho_Z(\mathbf{r})] - F_{ideal}^{ion}[\rho_B(\mathbf{r})] - \mu(\rho_0)\int d\mathbf{r}[\rho_Z(\mathbf{r}) - \rho_Z(\mathbf{r})]$$
$$= k_B T \int d\mathbf{r}\rho_Z(\mathbf{r})[\ln\{\lambda^3\rho_Z(\mathbf{r})\} - 1] - k_B T \int d\mathbf{r}\rho_B(\mathbf{r})[\ln\{\lambda^3\rho_Z(\mathbf{r})\} - 1]$$
$$- k_B T \Delta N \ln(\lambda^3\rho_0) \quad (5)$$

where $\rho_B(\mathbf{r})$ (or $\rho_Z(\mathbf{r})$) is the counter ion density of the B-DNA (or Z-DNA) solution, and ΔN denotes the number of ions in the Z-DNA solution minus that of ions in the B-DNA solution sphere. The relation for the chemical potential $\mu = k_B T \ln(\lambda^3 \rho_0)$ is used.[38]

Results and Discussion

Stability of MD Simulations. MD trajectories of B-DNA and Z-DNA in 0.1 M and 5 M salt solutions were examined to check for stability of the individual simulations. As shown in Figure 2, rmsd (root-mean-square deviation) from the initial structure converged to 2.3 Å for B-DNA and 1.2 Å for Z-DNA at the 0.1 M salt concentration, and to 2.1 Å for B-DNA and 1.1 Å for Z-DNA at 5 M salt. The average atomic fluctuations (calculated excluding hydrogen atoms and the terminal nucleotide atoms) were 1.45 Å for B-DNA and 0.87 Å for Z-DNA at 0.1 M and 1.46 Å for B-DNA and 0.90 Å for Z-DNA at 5 M. The observations of trajectory convergence and stability demonstrate the ability of parmbsc0 force field to reproduce the DNA conformations in the current set of simulations.[41] The larger fluctuations for B-DNA compared to those for Z-DNA verify that Z-DNA is structurally more rigid than B-DNA at both low and high salt concentrations.[42]

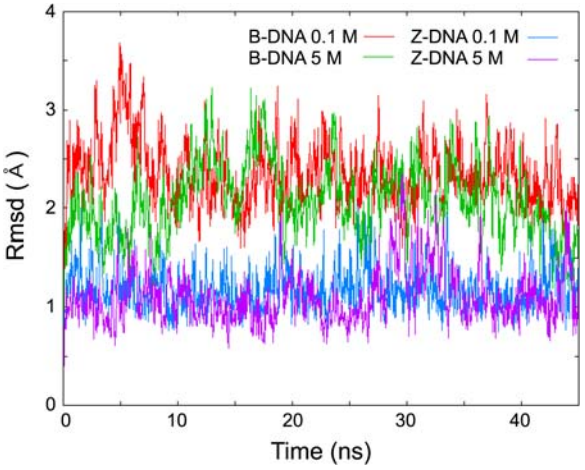

Figure 2. Root-mean-square deviations (rmsd) from the initial B-DNA and Z-DNA conformations are plotted as a function of simulation time for each of the four indicated simulations.

Change of DNA Conformations with Salt Concentration. Changes in DNA conformations were observed for different salt concentrations. B-DNA showed more significant changes in the phosphate-deoxyribose backbone conformation with the change in salt concentration than those in Z-DNA. For example, the deoxyribose ring pucker phase angle of dC in B-DNA showed a significant change (6.5°) with concentration, which supports earlier report of cytosine ribose flexibility in B-DNA.[22,43] In addition to these changes in local parameters, other structural changes such as global helical parameters are described in Supporting Information.

Free Energy Difference between B-DNA and Z-DNA Estimated from MM-PBSA. The MM-PBSA analysis results are summarized in Table 1. The B-DNA exhibits a lower gas phase mechanical energy ($\langle H_{int}+H_{vdW}+H_{Coul}\rangle$) than Z-DNA at both 0.1 M and 5 M salt concentrations, as expected based on the more favorable Coulomb electrostatic interaction energy (H_{Coul}) in B-DNA than in Z-DNA. Z-DNA exhibits larger electrostatic repulsion between closely-located negatively-charged phosphate groups. Although Z-DNA has a more favorable van der Waals energy (H_{vdW}) value due to its compact structure, it has more internal strain (H_{int}) due to its non-canonical structure. The entropy term ($-T\Delta S$), which is composed of translation, rotation, and vibration entropy, is larger for B-DNA than Z-DNA. That result reflects the higher relative flexibility in B-DNA observed in the MD simulation trajectories. The magnitude of the entropy value agrees with that in previous report of 1.08 kcal/mol per base-pair.[44]

In contrast to the mechanical energy calculation results, the PB-based calculation indicate that Z-DNA is more stabilized through solvation than B-DNA; thus, resulting in the lower free energy for the Z-form at both 1 M and 5 M salt concentrations. However, this does not agree with experimental observations that B-DNA is more favored at low salt condition.[9,10] Similar observations, in which the electrostatic contributions obtained from non-linear PB calculations explained the stability of Z-DNA at a high salt concentration but failed to explain the stability of B-DNA at a low concentration, have been reported.[19] That report suggested that conformational entropy was responsible for the relative stability of B-DNA at low salt concentration. Here,

Table 1. The MM-PBSA derived free energy components of B-DNA and Z-DNA at 0.1 M and 5 M NaCl concentrations

Free energy components	0.1 M			5 M		
	B-DNA	Z-DNA	Difference (Z-B)	B-DNA	Z-DNA	Difference (Z-B)
$\langle H_{Coul}\rangle$	-230.64	642.87	873.51	-222.26	724.23	946.49
$\langle H_{vdW}\rangle$	-205.92	-242.11	-36.19	-208.56	-243.49	-34.93
$\langle H_{int}\rangle$	1114.39	1133.39	19.00	1112.99	1134.45	21.46
$\langle G_{SA}\rangle$	26.70	24.68	-2.02	26.52	24.54	-1.98
$\langle G_{PB}\rangle$	-6331.43	-7205.73	-874.30	-6337.65	-7293.98	-956.33
$-T\langle S\rangle$	-625.55	-610.57	14.98	-625.15	-610.43	14.72
Sum	-6252.44	-6257.46	-5.02 (0.74[a])	-6254.10	-6264.67	-10.57 (0.76[a])

[a]Standard error. All values are in kcal/mol.

however, concentration-dependence of the entropy change was small (Table 1).

Many possible sources of the discrepancies between the above MM-PBSA results and the experimental results can be suggested, including errors in the force field, inherent approximations in the PBSA solvation model, and ignorance of counterion entropy. It has been suggested that a PB implicit solvation model exhibits too large a localization of solvent polarization in highly charged regions[25,27] because the finite size of the solvent molecules and the nonlocal communication among solvent molecules are not considered in the model. This localization tendency can be reduced by calibration of van der Waals radius parameters[27]; however, this was not attempted in this study. The calculations related to the salt ions in the PB model can also be problematic because of their finite size and the presence of correlations between ions.

Pair-wise Decomposition of the Free Energy Difference between B-DNA and Z-DNA. Regardless of the potential errors within the MM-PBSA calculations, we conducted a free energy decomposition analysis to determine if different substructure interactions would stabilize Z-DNA at a high salt concentration; for example, interactions between Watson-Crick (WC) base-pairs and base-pair stacking interactions were assessed.

As can be seen from Supporting Information Table S3, the largest contribution to the difference between the B-DNA and Z-DNA free energies is from the dC-dG interactions in the CpG step (-4.16 kcal/mol per step for the two such interactions in each step). Table S4 shows that this Z-DNA stability comes from the dC backbone-dG interaction (-4.63 kcal/mol). Re-examination of the interaction geometry of Z-DNA indicates that the deoxyribose ring of dC and the base of dG are closely located (Figure S2). Such Z-DNA stabilizing interactions have also been discussed in previous quantum chemical studies.[45-47] The current decomposition results reinforce the suggestion that dC-dG packing in the CpG step plays an important role in the relative stability of Z-DNA over B-DNA in high salt concentration. The results do not support the roles of π-π base packing or hydrogen bonding in DNA stability, both of which are commonly discussed as important factors in DNA stability.

Cation Distributions Around B-DNA and Z-DNA. In our MD simulations, the counterions around the DNA showed characteristic localized distribution patterns depending on the DNA conformation (Figure 3). Several sodium cations were observed to remain close to the phosphate groups in both B-DNA and Z-DNA. Because all of the cations that were closest to DNA phosphate groups were within 3 Å of the phosphate group, there is no doubt that phosphate regions are strong interaction sites for cations. Our simulations also show that the B-DNA major groove and the Z-DNA minor groove provide ionophores, observations that support those in previous reports.[23,24] Locations of the cations are illustrated in Figure 3.

The ion localization patterns are depicted in Figure 4 as ions distributed along the helical axis (*z*-axis) and azimuth (θ) planes, at different distances from the helical axis. The figure shows that the correlations between the ion distribution patterns and DNA structural features tend to decrease with increasing radial distance (distances indicated by i, ii, and iii in Figure 4(c)).

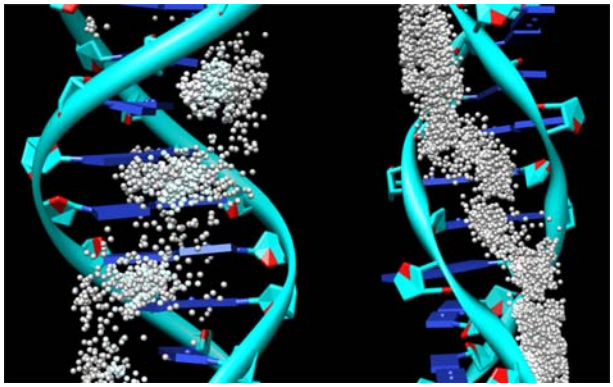

Figure 3. Localization of Na^+ ions in the major groove of B-DNA (left) and in the minor groove of Z-DNA (right) at 0.1 M NaCl concentration are illustrated in average DNA structures. Grey-white circles represent the cation positions sampled during MD simulations. For clarity, only ions located 0-6 Å from the helical axis are shown.

As shown in the B-DNA simulations in Figure 3 (left), the cations mainly located near the major groove along the helical axis between the C-G pairs in the GpC step, with less localization of cations in the CpG step. This alternating occupation of the base steps is also observed in Figure 4(c), (left (i)) at both 0.1 M and 5 M salt concentrations. In addition, the aforementioned convergence in the MD simulations is supported by the similar densities of ions at the equivalent sites in Figure 4(c). A similar, but weak cation distribution pattern around the major groove is also present around Z-DNA (Figure 4(c, right (ii))). However, at both low and high salt concentrations, ions near Z-DNA are concentrated to a greater extent in the minor groove (Figure 4(c)), due to the proximity of phosphate groups in that groove.

The differences in the densities of the dots in Figure 4(c) (i) and (ii), and in the heights of the ion density profiles in Figure 5, indicate that counterions located near Z-DNA exhibit a higher degree of ordering than those near B-DNA in the 0.1 M salt solution. For example, the highest local density around Z-DNA is about 9 times the average density, whereas it is about 4 times the average density for B-DNA. In contrast, no such marked difference between B-DNA and Z-DNA is observed in the 5 M salt solution.

Counterion Entropy Estimated Using the Molecular Density Functional Theory. Several methods may be used to relate the above observations on the different degrees of counterion ordering around B-DNA and Z-DNA at different salt concentrations to counterion entropy. Here, we employed molecular DFT, which has a functional form simplicity that is based on local ion density. The DFT approach considers both finite ion sizes and ion-ion correlations by using an ion density profile obtained from all-atom simulations. Here, DFT formalism is applied to the MD simulation results

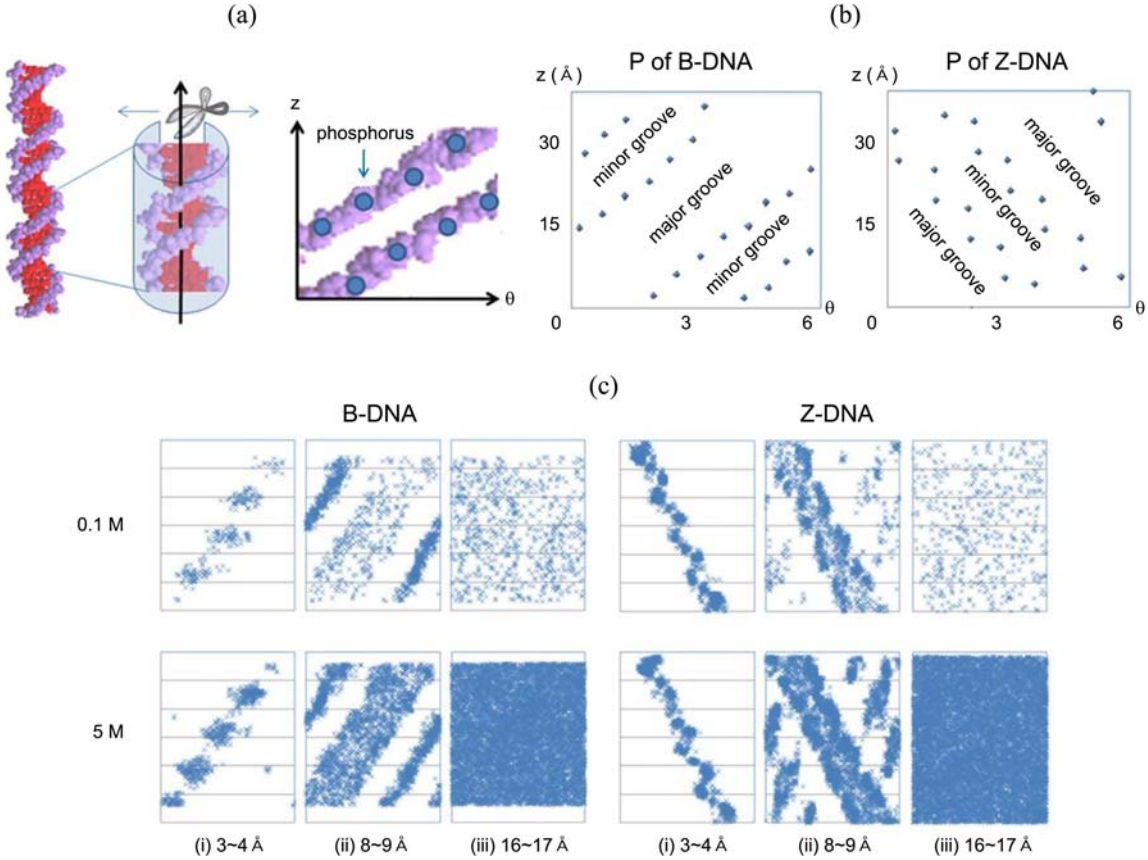

Figure 4. Changes in ion distribution with distance from the helical axis for B-DNA and Z-DNA at 0.1 M and 5 M salt concentrations. Definition of the cylindrical coordinate system is illustrated in (a). The locations of the DNA phosphorus (P) atoms shown in (a) are plotted in (b), which also shows the locations of the major and minor grooves. These P atoms are located ~9 Å from the helical axis. The ion positions collected from the 1,500 snapshots from the MD simulation trajectories are plotted in (c) for B-DNA (left) and Z-DNA (right). Ion positions are shown at three different ranges of radial distance (Å).

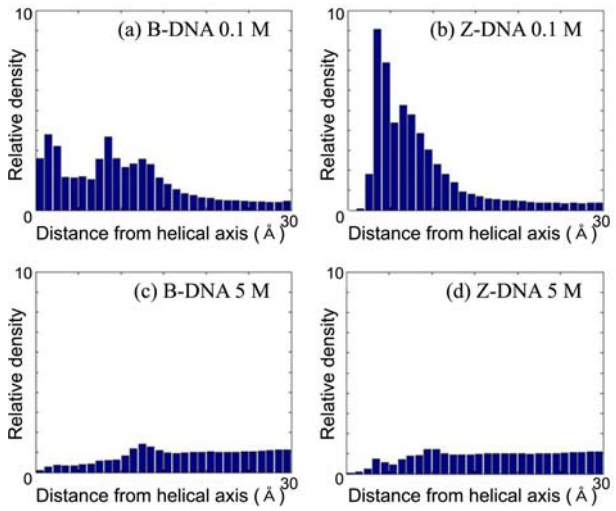

Figure 5. Relative ion density profiles along the radial axis for B-DNA and Z-DNA in 0.1 M and 5 M NaCl solutions. The Y-axis denotes relative ion density, which is local density divided by the average density.

by extending those simulation results to bulk solutions (see Methods).

The obtained counterion entropy estimates are summarized in Table 2, which shows that the entropy for B-DNA is more favorable than that for Z-DNA, consistent with the observations of less localized cation distribution around B-DNA, both at low and high salt conditions (Figure 5). The differential counterion entropy effect becomes less significant as salt concentration increases. Table 2 shows that at 0.1 M, ion ordering around Z-DNA is more pronounced than around B-DNA. It may be related to the short distance between phosphate groups across the minor groove of Z-DNA, which tighten the interactions between cations and DNA. In addition, the flexibility of B-DNA is expected to enhance the dispersal of the surrounding ions compared to the flexibility-related dispersal around stiffer Z-DNA. However, at 5 M, this differential entropy feature becomes weaker, presumab-

Table 2. The difference in free energy between B-DNA and Z-DNA calculated from MM-PBSA and the difference in counterion entropy calculated using a classical density functional theory. Values are in kcal/mol

Free energy difference	0.1 M	5 M
$G_Z - G_B$	-5.02	-10.57
$G_Z^{ion} - G_B^{ion}$	11.32	3.65
sum	6.30	-6.92

ly because the overall concentration provides a sufficiently large amount of counterions to stabilize DNA.

Although the MM-PBSA free energy calculations alone could not explain the stability of the B-DNA at low salt concentrations, the counterion entropy results, together with the free energy from MM-PBSA results, did provide qualitative agreement with previous experimental observations that a B-DNA to Z-DNA transformation occurs at high salt concentration.[9,20,48] The magnitudes of the enthalpy and entropy difference (ΔH and $-T\Delta S$, respectively) between B-DNA and Z-DNA in high salt condition can be compared to previous experimental data, assuming that total entropy is the sum of the translation, rotation, and vibration entropy of DNA and the counterion entropy, but ignoring the entropy contribution from the PBSA solvation free energy. The enthalpy and entropy differences are then ΔH = 2.11 and $-T\Delta S$ = 1.53 kcal/mol per base-pair, respectively, from our calculation and ΔH = 2.02 and $-T\Delta S$ = 1.05 kcal/mol per base-pair, respectively, in previous experiments.[17,20,48]

The free energy of Cl^- ions was computed in a similar manner, but the contribution was not as great as that of the Na^+ ions. The calculated Cl^- anion free energy difference between B-DNA and Z-DNA is 0.62 kcal/mol in the 5 M salt solution. Anion free energy was not calculated for the 0.1 M solution because the number of anions was too small (*i.e.*, 3 and 5 in the B-DNA and Z-DNA solution, respectively) to provide meaningful results.

The degree of counterion ordering is expected to be smaller for multivalent cations because, in such ions, a smaller number of ions would order around the DNA. Thus, the degree of counterion free energy can explain the observation that a B-Z DNA transition occurs at a lower salt concentration for divalent ions such as Mg^{2+} than for monovalent ions such as Na^+.[9]

Conclusion

The B-Z DNA transition at a high salt concentration indicates that DNA conformations are susceptible to environmental changes. In this study, we performed all-atom, explicit solvent MD simulations and estimated free energy components using MM-PBSA and DFT to explore the factors contributing to the B-Z DNA transition. In previous studies, the electrostatic part of the free energy estimates, derived using PB alone, could not explain the change the relative stability of B-DNA and Z-DNA in different salt concentrations,[19] even when the conformational entropy of DNA estimated using normal mode analysis was included. However, the results in this study suggest that changes in the relative stability of B-DNA and Z-DNA with salt concentration can be explained when the counterion free energy contribution originating from the relatively high ordering of cations around Z-DNA is considered. The effect of counterion entropy demonstrated implies that the exclusion of counterions by Z-DNA-binding proteins may be an important factor facilitating B-Z transitions in a variety of physiological conditions.

Our computations give results that are consistent with 3D-RISM based on integral equation theory,[11] and our approach allows decomposition of the relative contributions of different factors, including DNA entropy, counterion entropy, and the electrostatic portion of solvation free energy.

Acknowledgements. This work was supported by the National Research Foundation of Korea (NRF) grant funded by the Korean government (MEST) 2012-0001641.

References

1. Rich, A.; Nordheim, A.; Wang, A. *Annual Review of Biochemistry* **1984**, *53*, 791.
2. Rich, A.; Zhang, S. *Nature Reviews Genetics* **2003**, *4*, 566.
3. Wittig, B.; Dorbic, T.; Rich, A. *Proceedings of the National Academy of Sciences of the United States of America* **1991**, *88*, 2259.
4. Rahmouni, A.; Wells, R. *Science* **1989**, *246*, 358.
5. Takaoka, A.; Wang, Z.; Choi, M.; Yanai, H.; Negishi, H.; Ban, T.; Lu, Y.; Miyagishi, M.; Kodama, T.; Honda, K. *Nature* **2007**, *448*, 501.
6. Boehm, T.; Mengle-Gaw, L.; Kees, U.; Spurr, N.; Lavenir, I.; Forster, A.; Rabbitts, T. *The EMBO Journal* **1989**, *8*, 2621.
7. Thandla, S.; Ploski, J.; Raza-Egilmez, S.; Chhalliyil, P.; Block, A.; de Jong, P.; Aplan, P. *Blood* **1999**, *93*, 293.
8. Wang, G.; Christensen, L.; Vasquez, K. *Proceedings of the National Academy of Sciences* **2006**, *103*, 2677.
9. Behe, M.; Felsenfeld, G. *Proceedings of the National Academy of Sciences of the United States of America* **1981**, *78*, 1619.
10. Ramstein, J.; Leng, M. *Nature* **1980**, *288*, 413.
11. Maruyama, Y.; Yoshida, N.; Hirata, F. *J. Phys. Chem. B* **2010**, 375.
12. Klement, R.; Soumpasis, D.; Kitzing, E.; Jovin, T. *Biopolymers* **2004**, *29*, 1089.
13. Kollman, P.; Weiner, P.; Quigley, G.; Wang, A. *Biopolymers* **1982**, *21*, 1945.
14. Matthew, J.; Richards, F. *Biopolymers* **1984**, *23*, 2743.
15. Gueron, M.; Demaret, J. *Proceedings of the National Academy of Sciences* **1992**, *89*, 5740.
16. Gueron, M.; Demaret, J.; Filoche, M. *Biophysical Journal* **2000**, *78*, 1070.
17. Wereszczynski, J.; Andricioaei, I. *J. Phys. Chem. B* **2010**, 62.
18. Ponomarev, S.; Thayer, K.; Beveridge, D. *Proceedings of the National Academy of Sciences of the United States of America* **2004**, *101*, 14771.
19. Misra, V.; Honig, B. *Biochemistry* **1996**, *35*, 1115.
20. Tashiro, R.; Sugiyama, H. *Angewandte Chemie* **2003**, *115*, 6200.
21. Behe, M.; Felsenfeld, G.; Szu, S.; Charney, E. *Biopolymers* **2004**, *24*, 289.
22. Holak, T.; Borer, P.; Levy, G.; Van Boom, J.; Wang, A. *Nucleic Acids Research* **1984**, *12*, 4625.
23. Hud, N.; Polak, M. *Current Opinion in Structural Biology* **2001**, *11*, 293.
24. Howerton, S.; Sines, C.; VanDerveer, D.; Williams, L. *Biochemistry* **2001**, *40*, 10023.
25. Gavryushov, S.; Zielenkiewicz, P. *Biophysical Journal* **1998**, *75*, 2732.
26. Grochowski, P.; Trylska, J. *Peptide Science* **2008**, *89*, 93.
27. Dong, F.; Wagoner, J.; Baker, N. *Physical Chemistry Chemical Physics: PCCP* **2008**, *10*, 4889.
28. Bansal, M.; Bhattacharyya, D.; Ravi, B. *Bioinformatics* **1995**, *11*, 281.
29. Wang, A.; Quigley, G.; Kolpak, F.; Van der Marel, G.; Van Boom, J.; Rich, A. *Science* **1981**, *211*, 171.
30. Case, D. A.; Darden, T. A.; Cheatham, T. E., III; Simmerling, C. L.; Wang, J.; Duke, R. E.; Luo, R.; Crowley, M.; Walker, R. C.;

Zhang, W.; Merz, K. M.; Wang, B.; Hayik, S.; Roitberg, A.; Seabra, G.; Kolossváry, I.; Wong, K. F.; Paesani, F.; Vanicek, J.; Wu, X.; Brozell, S. R.; Steinbrecher, T.; Gohlke, H.; Yang, L.; Tan, C.; Mongan, J.; Hornak, V.; Cui, G.; Mathews, D. H.; Seetin, M. G.; Sagui, C.; Babin, V.; Kollman, P. A. *AMBER10*; University of California, San Francisco, 2008.
31. Perez, A.; Marchan, I.; Svozil, D.; Sponer, J.; Cheatham, T.; Laughton, C.; Orozco, M. *Biophysical Journal* **2007**, *92*, 3817.
32. Joung, I.; Cheatham, T. *J. Phys. Chem. B* **2008**, *112*, 9020.
33. Darden, T.; York, D.; Pedersen, L. *J. Chem. Phys.* **1993**, *98*, 10089.
34. Berendsen, H.; Postma, J.; Van Gunsteren, W.; DiNola, A.; Haak, J. *J. Chem. Phys.* **1984**, *81*, 3684.
35. Lavery, R.; Moakher, M.; Maddocks, J.; Petkeviciute, D.; Zakrzewska, K. *Nucleic Acids Research* **2009**.
36. Luo, R.; David, L.; Gilson, M. *Journal of Computational Chemistry* **2002**, *23*, 1244.
37. Sitkoff, D.; Sharp, K.; Honig, B. *J. Phys. Chem.* **1994**, *98*, 1978.
38. Oxtoby, D. W.; Evans, R. *J. Chem. Phys.* **1988**, 7521.
39. Seok, C.; Oxtoby, D. W. *J. Chem. Phys.* **1998**, 7982.
40. Oxtoby, D. W. *Crystallization of Liquids: A Density Functional Approach Liquids Freezing and Glass Transition*, 1990.
41. Perez, A.; Lankas, F.; Luque, F.; Orozco, M. *Nucleic Acids Research* **2008**, *36*, 2379.
42. Thomas, T.; Bloomfield, V. *Nucleic Acids Research* **1983**, *11*, 1919.
43. Duchardt, E.; Nilsson, L.; Schleucher, J. *Nucleic Acids Research* **2008**, *36*, 4211.
44. Irikura, K.; Tidor, B.; Brooks, B.; Karplus, M. *Science* **1985**, *229*, 571.
45. Escudero, D.; Estarellas, C.; Frontera, A.; Quinonero, D.; Deya, P. *Chem. Phys. Lett.* **2009**.
46. Egli, M.; Gessner, R. *Proceedings of the National Academy of Sciences of the United States of America* **1995**, *92*, 180.
47. Sponer, J.; Gabb, H.; Leszczynski, J.; Hobza, P. *Biophysical Journal* **1997**, *73*, 76.
48. Chaires, J.; Sturtevant, J. *Biopolymers* **1988**, *27*, 1375.